UC Irvine
UC Irvine Previously Published Works

Title
Air/Sea Transfer of Highly Soluble Gases Over Coastal Waters

Permalink
https://escholarship.org/uc/item/5fk9m9br

Journal
Geophysical Research Letters, 47(4)

ISSN
0094-8276

Authors
Porter, JG
Bruyn, WJ
Miller, SD
et al.

Publication Date
2020-02-28

DOI
10.1029/2019gl085286

Peer reviewed

Air/sea transfer of highly soluble gases over coastal waters

J. G. Porter[1], W. J. DeBruyn[2], S. D. Miller[3], and E. S. Saltzman[1]

[1]Departments of Earth System Science and Chemistry, University of California, Irvine, Irvine, California.

[2]Department of Chemistry and Biochemistry, Chapman University, Orange, California.

[3]Atmospheric Sciences Research Center, State University of New York at Albany, Albany, NY.

Corresponding author: Eric Saltzman (esaltzma@uci.edu)

Key Points:

- Direct flux measurements of sulfur dioxide to the coastal sea surface were made using eddy covariance.

- Simultaneous measurements of air/sea exchange of sulfur dioxide and water vapor show a difference in air-side resistance likely related to the molecular diffusivities of the two gases.

- These field measurements can be used to quantify the relative importance of molecular diffusion and turbulence in controlling soluble gas deposition to the sea surface.

Abstract

The deposition of soluble trace gases to the sea surface is not well studied due to a lack of flux measurements over the ocean. Here we report simultaneous air/sea eddy covariance flux measurements of water vapor, sulfur dioxide (SO_2), and momentum from a coastal North Atlantic pier. Gas transfer velocities were on average about 20% lower for SO_2 than for H_2O. This difference is attributed to the difference in molecular diffusivity between the two molecules ($D_{SO2}/D_{H2O} = 0.5$), in reasonable agreement with bulk parameterizations in air/sea gas models. This study demonstrates that it is possible to observe the effect of molecular diffusivity on air-side resistance to gas transfer. The slope of observed relationship between gas transfer velocity and friction velocity is slightly smaller than predicted by gas transfer models, possibly due to wind/wave interactions that are unaccounted for in current models.

1 Introduction

Research on air/sea exchange of trace gases has focused in recent years primarily on climate-active gases such as carbon dioxide, nitrous oxide, methane, and dimethylsulfide. These gases are moderately to slightly soluble in seawater and the physical processes controlling resistance to air/sea gas transfer for such gases occur mainly on the ocean side of the interface (Liss and Slater, 1974). Many highly soluble trace gases are generated by the atmospheric photochemical oxidation of natural and anthropogenic emissions. These include various inorganic acids (HCl, HNO_3, H_2SO_4), ammonia, and organic alcohols and acids. Such compounds also play important roles in biogeochemical cycles, climate, and air quality. Atmospheric water vapor, a major component of earth's energy budget, can also be considered a highly soluble gas.

There have been numerous theoretical and laboratory studies of soluble trace gas deposition to the sea surface, but few field studies (Garratt & Hicks, 1973; Hicks & Liss, 1976; Slinn et al., 1978; Joffre, 1988; Kramm & Dlugi, 1994). Direct flux measurements of soluble trace gases are challenging, due to low ambient concentrations and high reactivity with inlet tubing and other surfaces. The existing database of eddy covariance air/sea flux measurements for such gases consists of limited studies of acetone (Marandino et al., 2005; Yang et al., 2014), methanol (Yang et al., 2013; 2016), and SO_2 (Faloona et al. 2009, Porter et al., 2018). SO_2 is only moderately soluble but undergoes rapid hydrolysis and ionization in seawater and therefore behaves as a highly soluble gas during air/sea gas transfer (Liss, 1971; Millero et al., 1989; Porter et al., 2018). Deposition of SO_2 to the sea surface is a major component of the global sulfur cycle (Sheng et al., 2015).

The air/sea flux of a trace gas is related to the ocean/atmosphere concentration difference and to a gas transfer velocity. The bulk air/sea flux parameterization can be written as follows:

$$F = k \cdot (\frac{C_w}{\alpha} - C_a) \tag{1}$$

where F is the air/sea flux (mol m^2 s^{-1}), k is the gas transfer velocity (m s^{-1}, expressed in air-side units), C_w and C_a are the bulk ocean and air side gas concentrations (mol m^{-3}), and α is the dimensionless solubility (C_w/C_a). The inverse of the gas transfer velocity, or resistance, r=1/k (s m^{-1}), is conceptually useful for assessing the contribution of various physical processes to gas transfer. For highly soluble, air-side controlled gases, resistance occurs predominantly on the atmospheric side of the interface (Liss, 1971; Liss and Slater, 1974). Over the ocean, this resistance arises predominantly from two physical processes, 1) turbulent eddy transport across the atmospheric surface layer, and 2) diffusive transport across a thin viscous or interfacial layer adjacent to the surface where turbulence is suppressed. The bulk parameterizations in current use are based on a combination of micrometeorological theory, field observations, and laboratory studies (Duce et al., 1991; Fairall et al., 2000; Johnson, 2010).

There are very few simultaneous observations of air/sea gas exchange for soluble compounds with different molecular diffusivities. Such studies are needed to explore the processes controlling the air-side resistance to gas transfer and to validate bulk parameterizations. Porter et al. (2018) recently reported simultaneous air/sea flux measurements of SO_2 and water vapor from Scripps pier and detected systematic differences in transfer velocities for the two gases. They suggested that such differences could be used to quantify the relative importance of diffusive and turbulent transport, and gain insight into the air/sea gas transfer process. In this study, we present a more extensive dataset comparing gas

transfer velocities for SO_2 and water vapor from a coastal pier off North Carolina in the North Atlantic Ocean.

2 Field site and methods

2.1 Study site and experimental setup

This study was conducted at the US Army Corps of Engineers Field Research Facility (FRF-UCASE) in Duck, North Carolina from March 16-April 24, 2015 (DOY 75-114). Field measurements were made from the FRF-USACE pier (36°11.04'N 75°44.70'W). The pier is 560 m long and oriented perpendicular to the coastline, at a heading of roughly 70° E. The observations were made at the end of the pier, where the nominal water depth is approximately 7 m and the tidal range varied from 1-1.5m over the course of this field study. The sensors and air inlets were mounted on a 3-m long boom extending seaward from a meteorological tower at the end of the pier. The boom height above the sea surface ranged from 8-10 m depending on the tide.

The parameters measured on the pier included: fast response 3-D winds (CSAT3), fast response water vapor (LI-7500), sea surface temperature (thermistor, Apogee SI-111 IR sensor), and atmospheric pressure, temperature, and relative humidity (Vaisala HMP45), whitecaps (by visible imagery), and sea surface height (by ultrasonic sensor) (see Table S1 for details). Wind speed and direction from an anemometer at 19.4m elevation on the pier tower and SST data from the pier were obtained from the NOAA National Data Buoy Center (Station DUKN7, #8651370, Duck Pier, NC). Significant wave height was obtained from a Waverider directional buoy at the pier (USACE Gauge ID 630). Continuous real-time measurements of SO_2 were made using negative ion chemical ionization mass spectrometry, using a laboratory quadrupole-based instrument described previously (Bell et al., 2013; Porter et al., 2018). A shed located on the end of the pier housed the sulfur dioxide detector, data acquisition electronics, pumps, flow controllers, and clean air generator.

The air intake for SO_2 was a ¼" O.D. Teflon PFA tube fitting attached to a Teflon TFE manifold (2.5x2.5x10 cm) where the air stream was combined with an internal standard described below (Dupont Co.). The air intake was located approximately 10 cm behind the sensing region of the sonic anemometer. The air stream used for SO_2 detection was dried at the inlet using two counter-flow Nafion membrane driers in series to minimize losses of SO_2 to the tubing walls. Air was drawn to the SO_2 detector through a ¼" O.D. PFA Teflon tube, 21 m in length. SO_2 was ionized in the presence of O_3 to form the SO_5^- ion (Thornton et al., 2002; Mohler et al., 1992) during passage of air over a ^{63}Ni beta emitting foil at 430 Torr.

An isotopically-labelled $^{34}SO_2$ internal standard was added to the air inlet. Quantification of ambient SO_2 was done by simultaneously monitoring the mass spectrometer signals from $^{32}SO_5^-$ and $^{34}SO_5^-$, m/z 112 and 114. The internal standard was delivered from a high pressure aluminum cylinder containing ppm-level $^{34}SO_2$. This internal standard was calibrated in the laboratory against the output of a gravimetrically-calibrated SO_2 permeation tube. The instrument blank was determined by periodically introducing a carbonate-treated filter to the inlet. Dry air mixing ratios of SO_2 were calculated from the measured m/z 112/114 ratio using the procedures described by Porter et al. (2018). The sensitivity of the instrument ranged from 200-250 cps pmol mol^{-1} SO_2. The limit of detection is estimated at 4 pmol mol^{-1}.

Analog data from the meteorological sensors and SO_2 instrument were recorded at 50 Hz using a multichannel data logger with a 20 Hz Butterworth filter and LabView software (National Instruments).

2.2 Data processing and flux calculations

Post-processing of the data was carried out using Matlab (Mathworks). The data was converted to geophysical units and subdivided into 13-minute intervals for computing mean quantities, variances, and air-sea fluxes. Winds for each interval were rotated such that the mean vertical and cross-stream winds were zero. Systematic differences in calibration were observed between the LICOR open path water vapor sensor and the Vaisala relative humidity sensor. Data from the two instruments were adjusted to a common (Vaisala) scale by regressing the mean water vapor molar density computed from each sensor. This adjustment ensured that air-sea fluxes and air-sea concentration differences were reported on the same calibration scale. Visible images were processed for whitecap detection using the method of Callaghan and White (2009).

Fluxes of SO_2, water vapor and momentum were calculated according to the following equations:

$$F_{SO2} = \overline{w'C'_{SO2}} \tag{2}$$

$$F_{H2O} = \overline{w'X'_{H2O}}\,\bar{\rho}_{dry} \tag{3}$$

$$F_{mom} = \overline{w'u'}\bar{\rho} \tag{4}$$

where F is flux, primed quantities are fluctuations about the mean, the overbar indicates the time average across a flux interval, w is the vertical wind, C_{SO2} is the atmospheric concentration of SO_2, X is the mole fraction of water vapor, ρ_{dry} is the dry air molar density, u is horizontal wind speed, and ρ is air density. A small correction was made to the SO_2 fluxes to account for the loss of high frequency fluctuations in the inlet tubing (Porter et al., 2018). The largest source of uncertainty in the fluxes was covariance on time scales of several minutes. An Ogive method was used to estimate this uncertainty for each flux interval.

The data were quality controlled by eliminating flux intervals with the following characteristics: 1) poor cospectral shape, as determined by comparison to Kaimal et al. (1972), 2) very small bulk air/sea differences of water vapor or SO_2 ($\Delta X_{H2O} < 10^{-3}$; <10 pmol mol^{-1} SO_2

), 3) mean wind directions outside of the sector from 20°W-140°E (roughly ±90 of the orientation of the pier).

Transfer velocities for flux intervals passing quality control were calculated following equations:

$$k_{SO2} = \frac{F_{SO2}}{\bar{\rho}_{dry}\bar{X}_{SO2}} \tag{5}$$

$$k_{H2O} = \frac{F_{H2O}}{(\bar{X}_{H2O} - \bar{X}_{sat})\bar{\rho}_{dry}} \tag{6}$$

$$k_{mom} = \frac{F_{mom}}{\bar{U}\ \bar{\rho}} \tag{7}$$

Where k is transfer velocity, X_{sat} is mole fraction of water vapor in equilibrium at the sea surface, and U is horizontal wind speed. Uncertainties in k were estimated by propagating the uncertainties in the fluxes and mean quantities.

There is some question as to whether the Kansas-type flux-profile relationships (Kaimal et al., 1972) apply to a coastal environment such as the Duck pier where horizontal heterogeneity is strong and internal boundary layers are prevalent. Grachev et al. (2018) presented an extensive set of meteorological measurements at several levels on the Duck pier tower during 2015. During on-shore flow with an unstable boundary layer, flux-variance relationships were consistent with Monin-Obhukov Similarity Theory (MOST) theory but flux-profile relationships were not. In that study, the lowest levels on the tower may have experienced flow distortion due to the pier itself. In our study, the sensors projected seaward from the pier by 3m, and the mean vertical angular deflection of the winds was less than 2° for in-sector winds. Due to the uncertainty in flux-profile relationships, the measured winds were not corrected for the small variations in measurement height associated with tidal change in water depth (± 1 m).

3 Results

3.1. Meteorological conditions during the study

Climatological winds at the Duck pier during April and May are southeasterly in the 5-10 m/s range. The site experiences a local sea breeze circulation with onshore flow during the day and offshore flow at night. Winds at the site are episodically influenced by synoptic scale weather patterns which typically occur on the time scale of a week. During such events, winds typically shift to a northerly direction, followed by a gradual return to southeasterly flow over several days. Selected time series data from the study are shown in Figures 1 and S1. Wind speeds typically peaked around 15 m s^{-1} early in frontal events and declined to 5-8 m s^{-1} as the events ended. Air temperatures declined rapidly during the events from about 20 to 10°C, typically to within a degree of the sea surface temperature. The conditions encountered during this study are typical of the site, and similar to observations made later in the year (October-November, 2015; Grachev et al., 2018). SO_2 varied from below detection to above 300 pmol mol^{-1} over the course of the study. SO_2 levels were elevated during frontal passages, reflecting transport of continental North American air. SO_2 levels were generally below 100 pmol mol^{-1} after frontal passages and during easterly flow.

3.1. Wind speed dependence of gas transfer

Transfer velocities for momentum, water vapor, and sulfur dioxide for Duck pier exhibit a roughly linear dependence on friction velocity (u_*) over a wind speed range from 3-12 m s^{-1} (Figure 2). An estimate of the average transfer coefficient (k/u_*) for each parameter is provided by the slopes of the linear regressions of k vs. u_* (± 1 s.e.). These were obtained using the subset of the full Duck data set for which the winds were in-sector and momentum, water vapor, and sulfur dioxide fluxes all passed quality control.

$$k_{mom}/u_* = 3.93 \pm 0.11 \tag{8}$$

$$k_{H2O}/u_* = 2.64 \pm 0.09 \tag{9}$$

$$k_{SO2}/u_* = 2.27 \pm 0.10 \tag{10}$$

Transfer coefficients for the two gases are significantly smaller than those for momentum. The relative magnitudes of the transfer coefficients ($k_{mom}/u_* >> k_{H2O}/u_* > k_{SO2}/u_*$) is consistent with the physical processes controlling deposition of soluble gases. The transfer of mass at the air/sea interface is limited by the combined resistance due to turbulence (away from the interface itself) and diffusion across the viscous sublayer next to the surface. By contrast, momentum can be transferred to the surface both via viscous stress and by pressure fluctuations for which there is no analog in mass transfer (Liu et al., 1979). For transitional

or rough surfaces where form drag is significant, k_{mom} should always be greater than k_{gas}. At very low wind speeds and smooth water surfaces where viscous stress dominates, one might expect the difference between k_{mom} and k_{gas} to decrease. This would be difficult to observe under field conditions because the air/sea fluxes become very small at low wind speeds. In the case of light winds and large swells, wave energy may cause the momentum flux to be upward, while SO_2 flux remains downward.

The observed transfer coefficient for water vapor is slightly larger than that for sulfur dioxide ($k_{H2O} > k_{SO2}$). The difference between k_{H2O} and k_{SO2} is significant at the 95% confidence interval. This relationship is expected given that the H_2O is a smaller molecule than SO_2, with a molecular diffusivity in air nearly twice that of SO_2 ($D_{H2O} = 0.25$; $D_{SO2} = 0.13$ $cm^2 \ s^{-1}$ at 298K; uncertainty estimated as $\pm 5\%$; Fuller et al., 1966; Hilsenrath, 1960; Andreas, 2005; Reid et al., 1987).

Physically-based bulk gas transfer parameterizations relate the gas transfer velocity (or resistance) to surface stress, which in turn is estimated from observables such as winds, waves, and air and sea surface temperatures. The calculation of surface stress from wind speed involves the calculation of surface roughness using a gravity-wave relationship such as the Charnock model, optimized for open ocean conditions. Such relationships often exhibit biases when compared to data from coastal environments, due to a variety of factors including thermal gradients, currents, fetch, land and ocean bottom topography, and surfactants (Smith, 1988; Brown et al., 2013; Geernaert et al., 1986). In order to compare gas transfer models to the Duck data set, we avoid such biases by using field observations of wind speed and momentum flux to specify friction velocity in the model calculations.

The Duck field data is compared to three gas transfer parameterizations which estimate the combined resistance from 1) the interfacial region where diffusion and viscosity are important, and the velocity profile is linear, and 2) the overlying turbulent layer where eddy diffusion dominates and the velocity profile is logarithmic. This is described simply as:

$$k_{a\_total}{}^{-1} = r_{a\_total} = r_{a\_interfacial} + r_{a\_turbulent} \qquad (11)$$

For smooth flow (smooth rigid wall or low wind speeds over a water surface) the velocity profile and resistance is well constrained by laboratory measurements (van Driest, 1956; Riley et al., 1982). In the rough flow regime, the velocity profile above a water surface is much more complex, and there is a lack of laboratory data for wind/wave conditions relevant to the ocean. The bulk parameterizations used here are from Duce et al. (1991; denoted as D1991), Fairall et al. (2000; 2011; COAREG3.6), Donelan and Soloviev (2016; denoted as DS2016).

The gas transfer models used here all exhibit near linear relationships between gas transfer velocities and friction velocity. For both water vapor and sulfur dioxide, the models exhibit a stronger dependence on wind stress than the observations. For water vapor, the model k/u* slopes are 25% (DS2016) and 50% (COAREG3.6, D1991) larger than the observations. The models match the H_2O observations well at intermediate winds, but are biased low at low winds and high at high winds (Figure 2). For SO_2, the models slopes are greater than the observed slope by 30% (COAREG 3.6 and DS2016) and 60% (D1991). All of the models are in general agreement with the observed k_{SO2} at low winds, but overestimate the observations at intermediate and higher winds. Although the high wind speed data in this study is limited, the results appear to indicate that the k_{SO2} and k_{H2O} are lower than expected at $u_* >= 0.3 \ m \ s^{-1}$, or wind speeds above about 7 m s^{-1}.

Although the current models do not predict non-linearity in the relationship between gas transfer velocity and wind stress for air-side controlled gases, there are physical reasons why it might occur. The mechanisms by which momentum is transferred to the sea surface change dramatically as a function of wind speed and sea state. Viscous (sometimes referred to as tangential) surface stress predominates at low wind speeds and form drag becomes dominant at intermediate and high wind speeds. Momentum is also transferred by wave breaking and associated air-flow separation can lead to sheltering of the wave troughs. The total stress at the surface has been described as the sum of viscous, wave-induced, and air flow separation components (Reul et al., 1999; Kondryavtsev & Makin, 2001; Mueller & Veron, 2008).

Wind-wave effects have long been recognized as a strong influence on the drag coefficient (Donelan et al., 2004), but have only recently received attention in gas transfer. Wind-wave effects were suggested to explain recent observations of suppressed gas transfer of dimethylsulfide at intermediate to high wind speeds (Yang et al., 2011; Bell et al., 2013; 2014; Blomquist et al., 2017, Zavarsky et al., 2015; Brumer et al., 2017). To simulate those effects, the COAREG model was modified to partition surface stress between viscous and wave-induced components in calculating water-side gas transfer resistance (Yang et al., 2011; Fairall et al., 2011). COAREG 3.6 follows Mueller and Veron (2009) in computing viscous stress as equivalent to the smooth flow limit, where roughness length, $z_0 = 0.11\nu/u_{*0}$. Here we apply the same partitioning to the wind stress in the calculation of air-side resistance, using the COAREG model as follows:

$$r_{a\,interfacial} = \frac{1}{u_{*\,tangential}} 13.3 * Sc^{1/2} \tag{12}$$

$$r_{a\,turbulent} = \frac{1}{u_{*\,total}}\left[C_d^{-1/2} + \frac{0.5*\log(Sc)}{0.4} - 5\right] \tag{13}$$

$$k_{a\,interfacial} = (r_{a\,interfacial} + r_{a\,interfacial})^{-1} \tag{14}$$

where Sc is Schmidt number (C_d is the drag coefficient. This approach greatly oversimplifies the complex dynamics of wind-wave interactions (e.g. Yang and Shen, 2017), but it illustrates how waves might alter the linearity of the wind speed dependence of soluble gas deposition. The wave-modified COAREG model shows the expected effect, that the wind speed-dependence of air-side resistance decreases with increasing wind speeds, which simulates the general character of the Duck data set better than the other models, with lower RMS errors for both the individual observations and the bin-averaged data (Fig. 2; Table S1). With more detailed field measurements of wave properties, this simplified approach could be extended by explicitly incorporating flow separation and wave sheltering, which might further suppress viscous stress.

3.2. Sc-number dependence of air-side resistance

Gas transfer across water surfaces scales as Sc^{-n}, where n lies in the range from 0.67 for smooth surfaces at very low wind speeds, to 0.5 for transitional and rough conditions (Jahne et al., 1987; Richter & Jahne, 2011). These values are based on gas transfer theory and laboratory studies of water-side controlled gases with lower solubilities and much larger Sc than the gases studied here. Nightingale et al. (2000) conducted the only oceanic field study of n using water-side controlled gases, reporting a value of $0.51^{+0.19}_{-0.14}$.

Sc_{SO2} in air is roughly twice that of H_2O ($Sc_{H2O}=0.61$, $Sc_{SO2}=1.19$ at 298 K) (Fuller et al., 1966; Hilsenrath, 1960). Simultaneous measurements of gas transfer velocities for water

vapor and SO_2 therefore have the potential to constrain the Sc-dependence of soluble gas transfer under field conditions. A total least squares regression of k_{SO2} against k_{H2O} for the Duck data set yields a slope of 0.81±0.04 (1 std. err.; Figure 3). A previous study at Scripps pier yielded a 0.62±0.24, with considerably larger uncertainty due to the limited size and wind speed range of those data (Porter et al., 2018). The Duck results are at the lower end of the range of 0.85-0.95 predicted by the gas transfer models introduced above.

The observed k_{SO2}/ k_{H2O} can be used to calculate an overall or "effective" Sc-dependence. For soluble gases, the observed Sc-dependence reflects the combined contributions of resistance in the viscous interfacial sublayer and in the overlying turbulent surface layer. The turbulent (or aerodynamic) resistance is a significant component of the total resistance for soluble gases and is assumed to have zero Sc dependence. Consequently, the effective Sc-dependence for soluble gases should be considerably smaller than that for water-side controlled gases where almost all of the resistance is located within the interfacial sublayer.

The effective Sc-dependence, denoted as m (to differentiate from n, the Sc-dependence of the interfacial sublayer itself), is calculated as follows:

$$\frac{k_{SO_2}/u_*}{k_{H_2O}/u_*} = \left(\frac{Sc_{SO_2}}{Sc_{H_2O}}\right)^{-m} \tag{15}$$

Substituting the regression slope of k_{SO2} against k_{H2O} (Fig. 3):

$$0.81 \pm 0.04 = \left(\frac{1.19}{0.61}\right)^{-m} \tag{16}$$

which yields m=0.32±0.07 (neglecting uncertainty in the diffusivities). The gas transfer models examined here (D91, COAREG, and DS16) predict slightly lower values of m, ranging from 0.08-0.24 (Figure 2). The mismatch implies that these models underestimate either 1) the fraction of total resistance in the interfacial sublayer compared to the turbulent layer (as discussed earlier), or 2) the Sc-dependence (n) of transport across the interfacial sublayer. The wave-modified COAREG model exhibits wind speed-dependence in m ranging from 0.29-0.36 for u_* ranging from 0.2-0.5. The Duck field data are insufficient to determine if the Sc-dependence varies with u_*. Lab studies suggest that the transition of n from smooth to rough values occurs over a broad range of u_*, and is sensitive to surfactants (Richter & Jahne, 2011; Nagel et al., 2019).

This study provides a field-based estimate of the dependence of air-side resistance on molecular diffusivity. Earlier studies obtained a similar trend in Sc-dependence for air/sea transfer of sensible heat and methanol (Sc = 0.64 and 1.09, respectively; Yang et al., 2013; 2014). Those result are dependent on the assumption that sea surface methanol levels were negligible, in spite of the presence in the underlying bulk seawater.

3.2. Conclusions

This study presents simultaneous eddy covariance flux measurements of water vapor and sulfur dioxide to the coastal sea surface. The data show that the gas transfer velocity for SO_2 is less than that for H_2O, as expected because of diffusive resistance to gas transfer in the interfacial layer just above the sea surface. The Duck field study confirms previous limited field observations at Scripps pier (Porter et al., 2018). The results are in qualitative agreement with gas transfer theory and bulk parameterizations of gas transfer of highly soluble gases. Quantitatively, the field data exhibit a Sc number dependence slightly greater than predicted by the models. The data also provides intriguing preliminary evidence for non-linearity in the relationship between the gas transfer velocities and friction velocity, that

we speculate results from wind-wave interactions. This study highlights the potential for simultaneous eddy covariance flux measurements of multiple highly soluble compounds to provide new insights into mass transfer across the air side of the air-sea interface.

References

Andreas, E. (2005). *Handbook of Physical Constants and Functions for Use in Atmospheric Boundary Layer Studies* (US Army Corps of Engineers No. ERDC/CRREL M-05-1) (p. 54).

Bell, T. G., De Bruyn, W., Miller, S. D., Ward, B., Christensen, K. H., & Saltzman, E. S. (2013). Air-sea dimethylsulfide (DMS) gas transfer in the North Atlantic: evidence for limited interfacial gas exchange at high wind speed. *Atmospheric Chemistry and Physics*, *13*(21), 11073–11087. https://doi.org/10.5194/acp-13-11073-2013

Bell, T. G., De Bruyn, W., Marandino, C. A., Miller, S. D., Law, C. S., Smith, M. J., & Saltzman, E. S. (2015). Dimethylsulfide gas transfer coefficients from algal blooms in the Southern Ocean. *Atmospheric Chemistry and Physics*, *15*(4), 1783–1794. https://doi.org/10.5194/acp-15-1783-2015

Blomquist, B. W., Brumer, S. E., Fairall, C. W., Huebert, B. J., Zappa, C. J., Brooks, I. M., et al. (2017). Wind speed and sea state dependencies of air-sea gas transfer: results from the high wind speed gas exchange study (HiWinGS). *Journal of Geophysical Research: Oceans*, *122*(10), 8034–8062. https://doi.org/10.1002/2017JC013181

Brown, J. M., Amoudry, L. O., Mercier, F. M., & Souza, A. J. (2013). Intercomparison of the Charnock and COARE bulk wind stress formulations for coastal ocean modelling. *Ocean Science*, *9*(4), 721–729. https://doi.org/10.5194/os-9-721-2013

Brumer, S. E., Zappa, C. J., Blomquist, B. W., Fairall, C. W., Cifuentes-Lorenzen, A., Edson, J. B., et al. (2017). Wave-related Reynolds number parameterizations of CO_2 and DMS transfer velocities. *Geophysical Research Letters*, *44*(19), 9865–9875. https://doi.org/10.1002/2017GL074979

Businger, J. A., Wyngaard, J. C., Izumi, Y., & Bradley, E. F. (1971). Flux-profile relationships in the atmospheric surface layer. *Journal of the Atmospheric Sciences*, *28*(2), 181–189. https://doi.org/10.1175/1520-0469(1971)028<0181:FPRITA>2.0.CO;2

Callaghan, A. H., & White, M. (2009). Automated Processing of Sea Surface Images for the Determination of Whitecap Coverage. *Journal of Atmospheric and Oceanic Technology*, *26*(2), 383–394. https://doi.org/10.1175/2008JTECHO634.1

Donelan, M. A., & Soloviev, A. V. (2016). A mixing length model for the aqueous boundary layer including the effect of wave breaking on enhancing gas transfer. *IOP Conference Series: Earth and Environmental Science*, *35*(1), 012001.

Duce, R. A., Liss, P. S., Merrill, J. T., Atlas, E. L., Buat-Menard, P., Hicks, B. B., et al. (1991). The atmospheric input of trace species to the world ocean. *Global Biogeochemical Cycles*, *5*(3), 193–259. https://doi.org/10.1029/91GB01778

Faloona, I., Conley, S. A., Blomquist, B., Clarke, A. D., Kapustin, V., Howell, S., et al. (2009). Sulfur dioxide in the tropical marine boundary layer: dry deposition and heterogeneous oxidation observed during the Pacific Atmospheric Sulfur Experiment. *Journal of Atmospheric Chemistry*, *63*(1), 13–32. https://doi.org/10.1007/s10874-010-9155-0

Fairall, C. W., Bradley, E. F., Rogers, D. P., Edson, J. B., & Young, G. S. (1996). Bulk parameterization of air-sea fluxes for Tropical Ocean-Global Atmosphere Coupled-Ocean Atmosphere Response Experiment. *Journal of Geophysical Research: Oceans*, *101*(C2), 3747–3764. https://doi.org/10.1029/95JC03205

Fairall, C. W., Hare, J. E., Edson, J. B., & McGillis, W. (2000). Parameterization and micrometeorological measurement of air-sea gas transfer. *Boundary-Layer Meteorology*, *96*(1), 63–106. https://doi.org/10.1023/A:1002662826020

Fairall, C. W., Bradley, E. F., Hare, J. E., Grachev, A. A., & Edson, J. B. (2003). Bulk Parameterization of Air-Sea Fluxes: Updates and Verification for the COARE Algorithm. *Journal of Climate*, *16*(4), 571–591. https://doi.org/10.1175/1520-0442(2003)016<0571:BPOASF>2.0.CO;2

Fairall, C. W., Yang, M., Bariteau, L., Edson, J. B., Helmig, D., McGillis, W., et al. (2011). Implementation of the Coupled Ocean-Atmosphere Response Experiment flux algorithm with CO2, dimethyl sulfide, and O3. *Journal of Geophysical Research: Oceans*, *116*(C4). https://doi.org/10.1029/2010JC006884

Fuller, E. N., Schettler, P. D., & Giddings, J. C. (1966). New method for prediction of binary gas-phase diffusion coefficients. *Industrial & Engineering Chemistry*, 58(5), 18–27. https://doi.org/10.1021/ie50677a007.

Garratt, J. R., & Hicks, B. B. (1973). Momentum, heat and water vapour transfer to and from natural and artificial surfaces. *Quarterly Journal of the Royal Meteorological Society*, *99*(422), 680–687. https://doi.org/10.1002/qj.49709942209

Geernaert, G. L., Katsaros, K. B., & Richter, K. (1986). Variation of the drag coefficient and its dependence on sea state. *Journal of Geophysical Research: Oceans*, *91*(C6), 7667–7679. https://doi.org/10.1029/JC091iC06p07667

Hicks, B. B., & Liss, P. S. (1976). Transfer of SO_2 and other reactive gases across the air-sea interface1. *Tellus*, *28*(4), 348–354. https://doi.org/10.1111/j.2153-3490.1976.tb00683.x

Hilsenrath, J. (1960). Tables of thermodynamic and transport properties of air, argon, carbon dioxide, carbon monoxide, hydrogen, nitrogen, oxygen, and steam. Pergamon Press.

Joffre, S. M. (1988). Modelling the dry deposition velocity of highly soluble gases to the sea surface. *Atmospheric Environment (1967)*, *22*(6), 1137–1146. https://doi.org/10.1016/0004-6981(88)90343-5

Johnson, M. T. (2010). A numerical scheme to calculate temperature and salinity dependent air-water transfer velocities for any gas. *Ocean Science*, *6*(4), 913–932. https://doi.org/10.5194/os-6-913-2010

Kramm, G., & Dlugi, R. (1994). Modelling of the vertical fluxes of nitric acid, ammonia, and ammonium nitrate. *Journal of Atmospheric Chemistry*, *18*(4), 319–357.

Kudryavtsev, V. N., & Makin, V. K. (2007). Aerodynamic roughness of the sea surface at high winds. *Boundary-Layer Meteorology*, *125*(2), 289–303. https://doi.org/10.1007/s10546-007-9184-7

Liss, P. (1971). Exchange of SO_2 between the atmosphere and natural waters. *Nature*, *233*(5318), 327. https://doi.org/doi:10.1038/233327a0

Liss, P., & G. Slater, P. (1974). Flux of gases across the air-sea interface. *Nature*, *247*, 181–184.

Liu, W. T., Katsaros, K. B., & Businger, J. A. (1979). Bulk Parameterization of Air-Sea Exchanges of Heat and Water Vapor Including the Molecular Constraints at the Interface. Journal of the Atmospheric Sciences, 36(9), 1722–1735. https://doi.org/10.1175/1520-0469(1979)036<1722:BPOASE>2.0.CO;2

Marandino, C. A., De Bruyn, W. J., Miller, S. D., Prather, M. J., & Saltzman, E. S. (2005). Oceanic uptake and the global atmospheric acetone budget. *Geophysical Research Letters*, *32*(15). https://doi.org/10.1029/2005GL023285

Millero, F. J., Hershey, J. B., Johnson, G., & Zhang, J.-Z. (1989). The solubility of SO_2 and the dissociation of H_2SO_3 in NaCl solutions. *Journal of Atmospheric Chemistry*, *8*(4), 377–389. https://doi.org/10.1007/BF00052711

Möhler, O., Reiner, T., & Arnold, F. (1992). The formation of SO_5^- by gas phase ion-molecule reactions. *The Journal of Chemical Physics*, *97*(11), 8233–8239. https://doi.org/10.1063/1.463394

Mueller, J. A., & Veron, F. (2008). Nonlinear Formulation of the Bulk Surface Stress over Breaking Waves: Feedback Mechanisms from Air-flow Separation. *Boundary-Layer Meteorology*, *130*(1), 117. https://doi.org/10.1007/s10546-008-9334-6

Mueller, J. A., & Veron, F. (2008). Nonlinear Formulation of the Bulk Surface Stress over Breaking Waves: Feedback Mechanisms from Air-flow Separation. *Boundary-Layer Meteorology*, *130*(1), 117. https://doi.org/10.1007/s10546-008-9334-6

Nagel, L., Krall, K. E., & Jähne, B. (2019). Measurements of air–sea gas transfer velocities in the Baltic Sea. *Ocean Science*, *15*(2), 235–247. https://doi.org/10.5194/os-15-235-2019

Nightingale, P. D., Malin, G., Law, C. S., Watson, A. J., Liss, P. S., Liddicoat, M. I., et al. (2000). In situ evaluation of air-sea gas exchange parameterizations using novel conservative and volatile tracers. *Global Biogeochemical Cycles*, *14*(1), 373–387. https://doi.org/10.1029/1999GB900091

Oncley, S. P., Friehe, C. A., Larue, J. C., Businger, J. A., Itsweire, E. C., & Chang, S. S. (1996). Surface-layer fluxes, profiles, and turbulence measurements over uniform

terrain under near-neutral conditions. *Journal of the Atmospheric Sciences*, 53(7), 1029–1044. https://doi.org/10.1175/1520-0469(1996)053<1029:SLFPAT>2.0.CO;2

Porter, J. G., De Bruyn, W., & Saltzman, E. S. (2018). Eddy flux measurements of sulfur dioxide deposition to the sea surface. *Atmospheric Chemistry and Physics*, *18*(20), 15291–15305. https://doi.org/10.5194/acp-18-15291-2018

Reid, R. C., Prausnitz, J. M., & Poling, B. E. (1987). *The properties of gases of liquids: Their estimation and correlation. 4th Ed.* McGraw-Hill.

Sheng, J.-X., Weisenstein, D. K., Luo, B.-P., Rozanov, E., Stenke, A., Anet, J., et al. (2015). Global atmospheric sulfur budget under volcanically quiescent conditions: Aerosol-chemistry-climate model predictions and validation. Journal of Geophysical Research: Atmospheres, 120(1), 256–276. https://doi.org/10.1002/2014JD021985

Slinn, W. G. N., Hasse, L., Hicks, B. B., Hogan, A. W., Lal, D., Liss, P. S., et al. (1978). Some aspects of the transfer of atmospheric trace constituents past the air-sea interface. *Atmospheric Environment (1967)*, *12*(11), 2055–2087. https://doi.org/10.1016/0004-6981(78)90163-4

Smith, S. D. (1988). Coefficients for sea surface wind stress, heat flux, and wind profiles as a function of wind speed and temperature. *Journal of Geophysical Research: Oceans*, *93*(C12), 15467–15472. https://doi.org/10.1029/JC093iC12p15467

Thornton, D. C., Bandy, A. R., Tu, F. H., Blomquist, B. W., Mitchell, G. M., Nadler, W., & Lenschow, D. H. (2002). Fast airborne sulfur dioxide measurements by Atmospheric Pressure Ionization Mass Spectrometry (APIMS). *Journal of Geophysical Research: Atmospheres*, 107(D22), ACH 13-1. https://doi.org/10.1029/2002JD002289

Richter, K., & Jahne, B. (2011). A laboratory study of the Schmidt number dependency of air-water gas transfer. In *Gas Transfer at Water Surfaces 2010,* (pp. 322–332). Kyoto University Press. https://doi: 10.5281/zenodo.14955

Reul, N., Branger, H., & Giovanangeli, J.-P. (1999). Air flow separation over unsteady breaking waves. *Physics of Fluids*, *11*(7), 1959–1961. https://doi.org/10.1063/1.870058

Riley, D. S., Donelan, M. A., & Hui, W. H. (1982). An extended Miles' theory for wave generation by wind. *Boundary-Layer Meteorology*, *22*(2), 209–225. https://doi.org/10.1007/BF00118254

Van Driest E. R. (1956). On turbulent flow near a wall, *J. Aero. Sci.* 23(11), 1007-1011.

Yang, M., Blomquist, B. W., Fairall, C. W., Archer, S. D., & Huebert, B. J. (2011). Air-sea exchange of dimethylsulfide in the Southern Ocean: Measurements from SO GasEx compared to temperate and tropical regions. Journal of Geophysical Research: Oceans, 116(C4). https://doi.org/10.1029/2010JC006526

Yang, M., Nightingale, P. D., Beale, R., Liss, P. S., Blomquist, B., & Fairall, C. (2013). Atmospheric deposition of methanol over the Atlantic Ocean. *Proceedings of the National Academy of Sciences*, *110*(50), 20034–20039. https://doi.org/10.1073/pnas.1317840110

Yang, M., Beale, R., Liss, P., Johnson, M., Blomquist, B., & Nightingale, P. (2014). Air-sea fluxes of oxygenated volatile organic compounds across the Atlantic Ocean.

Atmospheric Chemistry and Physics, *14*(14), 7499–7517. https://doi.org/10.5194/acp-14-7499-2014

Zavarsky, A., Goddijn-Murphy, L., Steinhoff, T., & Marandino, C. A. (2018). Bubble-mediated gas transfer and gas transfer suppression of DMS and CO_2. *Journal of Geophysical Research: Atmospheres*, *123*(12), 6624–6647. https://doi.org/10.1029/2017JD028071
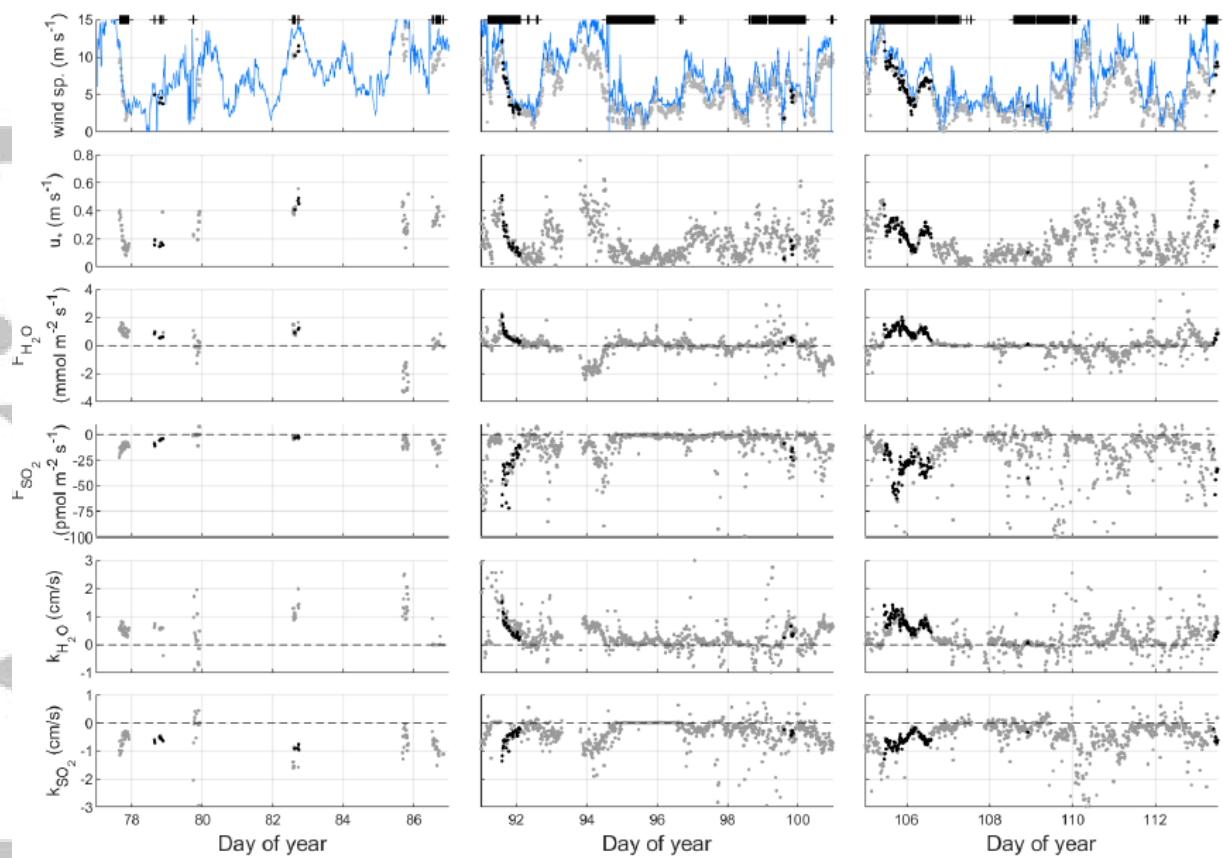
Figure 1. Time series observations from the FRF pier in Duck, North Carolina. For all panels - black points: intervals when k_{mom}, k_{H2O}, and k_{SO2} passed all quality control, gray points: intervals with data failing one or more quality control criteria. From top: 1) wind speed measured on the eddy covariance boom - + symbols across the top indicate intervals when winds were in-sector (on shore), blue line - FRF tower anemometer (30 m above mean sea level), 2) friction velocity calculated from observed momentum flux, 3) F_{H2O} – water vapor air/sea flux, 4) F_{SO2} – sulfur dioxide air/sea flux, 5) k_{H2O} – water vapor transfer velocity, , 6) k_{SO2} – sulfur dioxide transfer velocity. Time axis is in UTC.
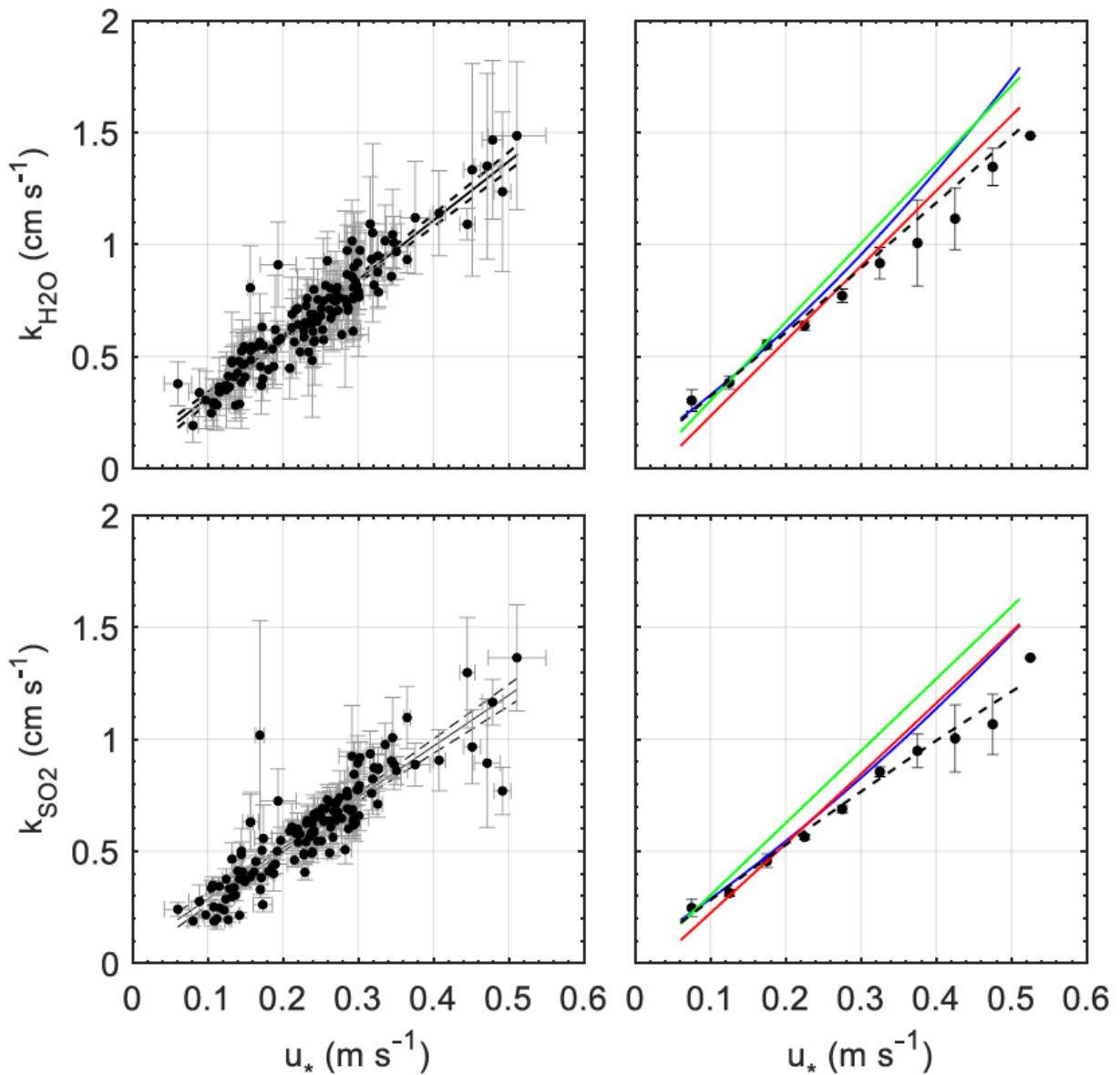
Figure 2. Simultaneous observations of gas transfer velocities as a function of friction velocity at the Duck pier, compared to several bulk gas transfer parameterizations. All measurements were made during onshore air flow. Upper row: water vapor, Bottom row: sulfur dioxide. Left plots: individual flux intervals with linear regression showing 95% confidence bounds (dashed line). Right plots: The same data bin-averaged by friction velocity in 0.05 m s^{-1} bins. The colored lines are from several air/sea gas transfer models, as follows (see text for abbreviations): COAREG 3.6 (blue), DS2016 (red), D1991 (green). The dashed black line is a wave-modified version of the COAREG 3.6 using only u$_{*tangential}$ to compute the air side interfacial resistance.
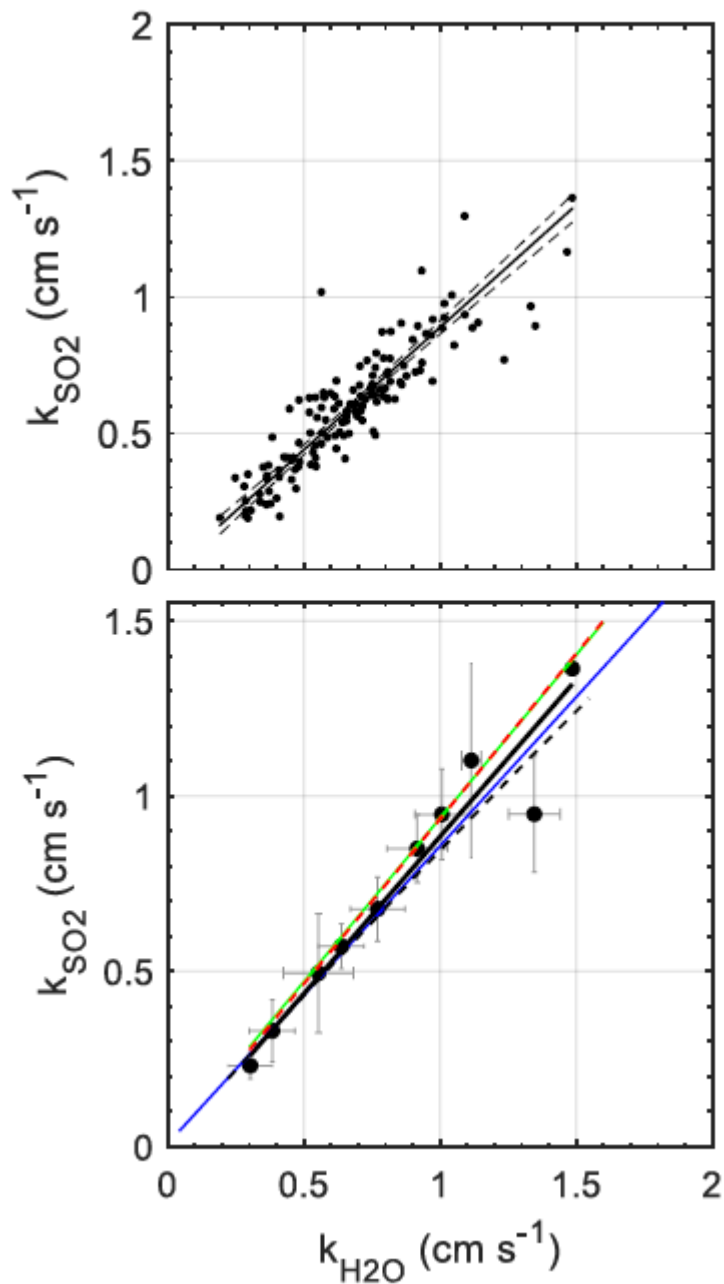
Figure 3. Gas transfer velocities of SO_2 and H_2O from simultaneous observations at the Duck pier during onshore air flow and neutral to unstable conditions, compared to gas transfer models. Upper: field observations. Lower: gas transfer velocities (mean±1σ) bin-averaged by u_* in 0.05 m s^{-1} bins. The black lines on both plots are total (two-way) linear regressions, with dashed upper and lower 95% confidence bounds. The colored lines are from air/sea gas transfer models, as follows (see text for abbreviations): COAREG 3.6 (blue), DS2016 (red dashed), D1991 (green). The dashed black line is a wave-modified version of the COAREG 3.6 using only $u_{*tangential}$ to compute the air side interfacial resistance.